Supporting Information

Ligand Impacts on Band Edge Energies and Excited State Splittings of Silicane

Guoying Yao,[1,2] Ekadashi Pradhan,[2] Zhenyu Yang,[1*] and Tao Zeng[2*]

[1]MOE Laboratory of Bioinorganic and Synthetic Chemistry, Lehn Institute of Functional Materials, School of Chemistry, IGCME, Sun Yat-Sen University, Guangzhou, Guangdong, 510275, China

[2]Department of Chemistry, York University, Toronto, Ontario, M3J 1P3, Canada

Corresponding E-mail: tzeng@yorku.ca; yangzhy63@mail.sysu.edu.cn

Section S1. Supplementary figures and tables for discussions in the main text

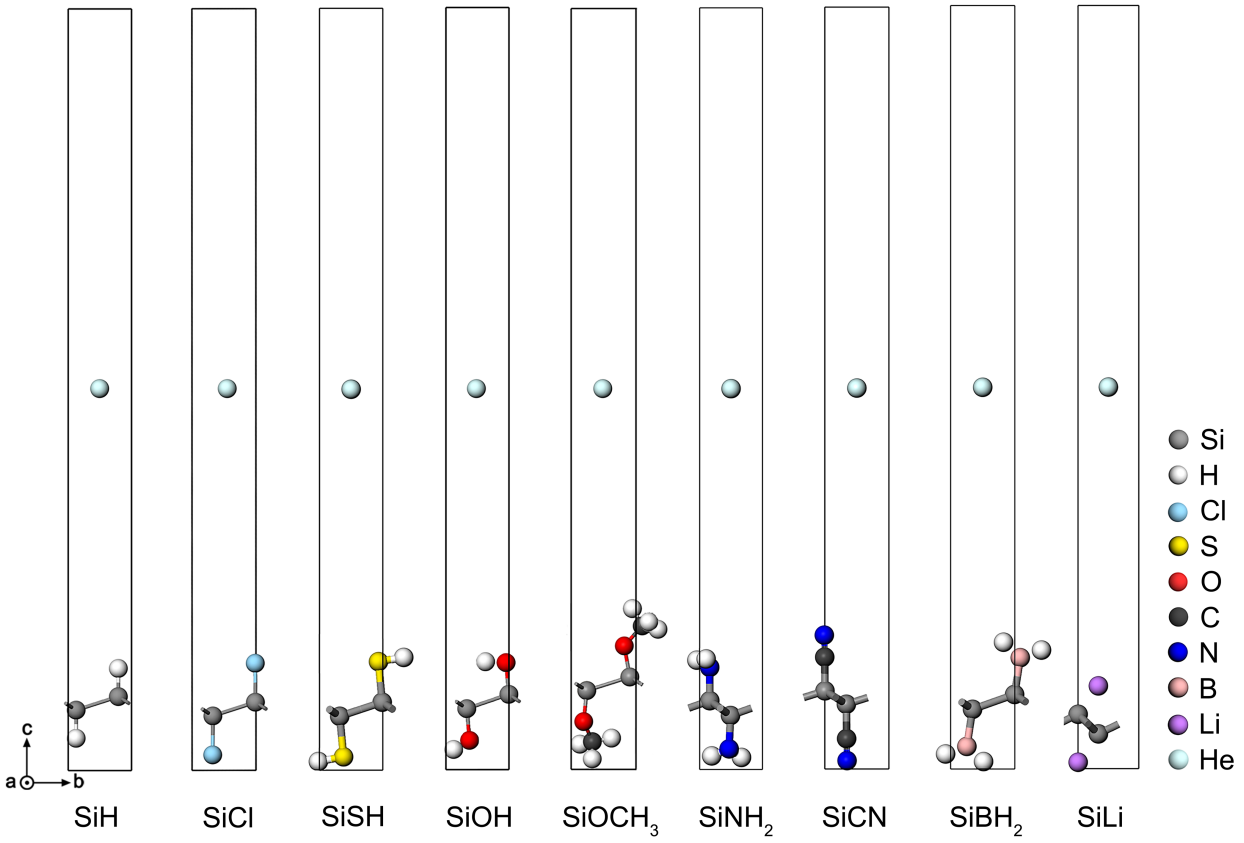

Figure S1. Unit cells of the models with one helium atom positioned 20 Å above the monolayer SiR species.

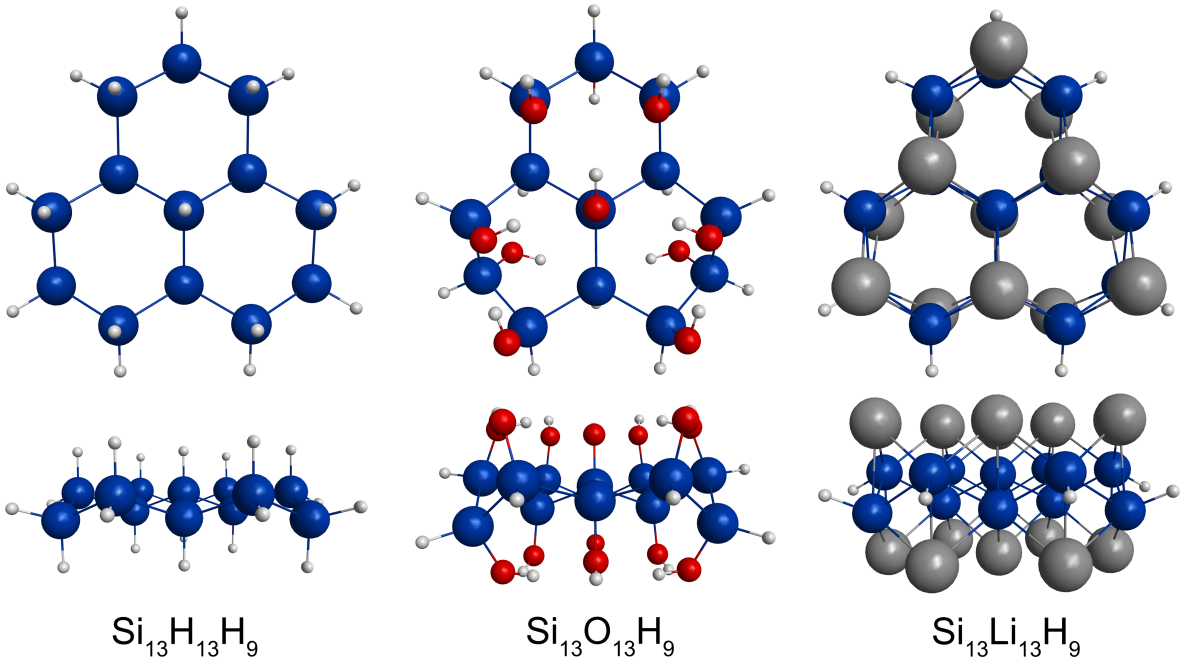

Figure S2. Top and side views of the $Si_{13}R_{13}H_9$ (R = H, OH, Li) molecular models for GAMESS-US calculations.

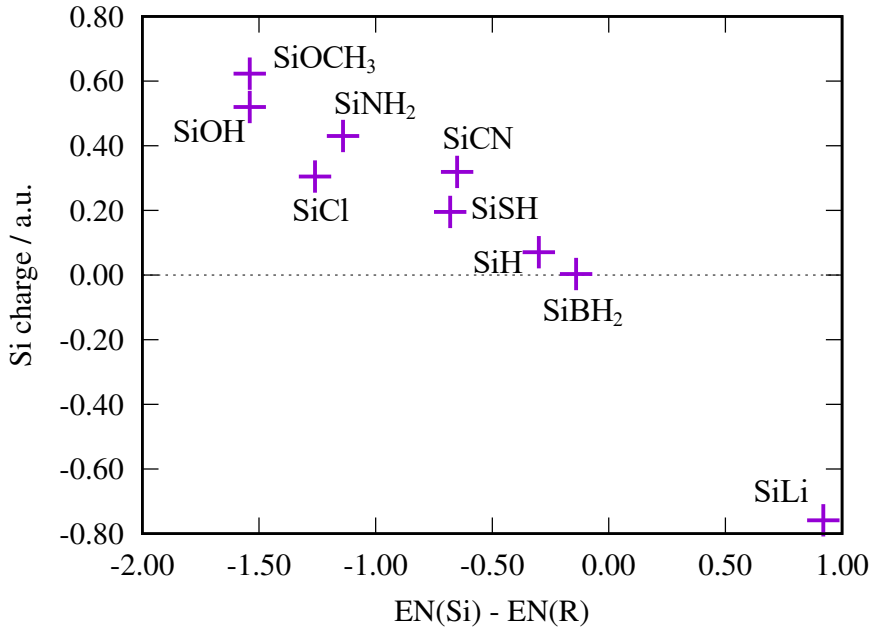

Figure S3. Anticorrelation between difference of electronegativities (EN) of Si and the ligand R and the Si atomic charge in SiR. Note that the electronegativity of the atom that is connected to Si is chosen to represent the electronegativity of R.

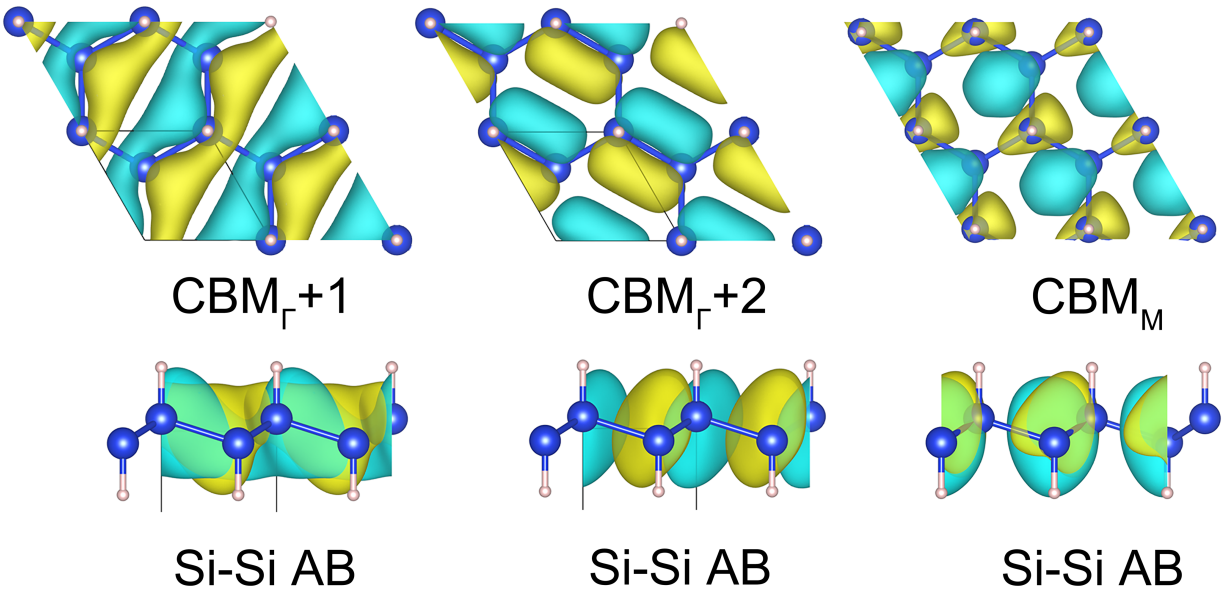

Figure S4. The periodic modulation functions of the CBM$_\Gamma$+1, +2, and CBM$_M$ orbitals for SiH.

"AB" means antibonding interaction between the denotated pair of atoms.

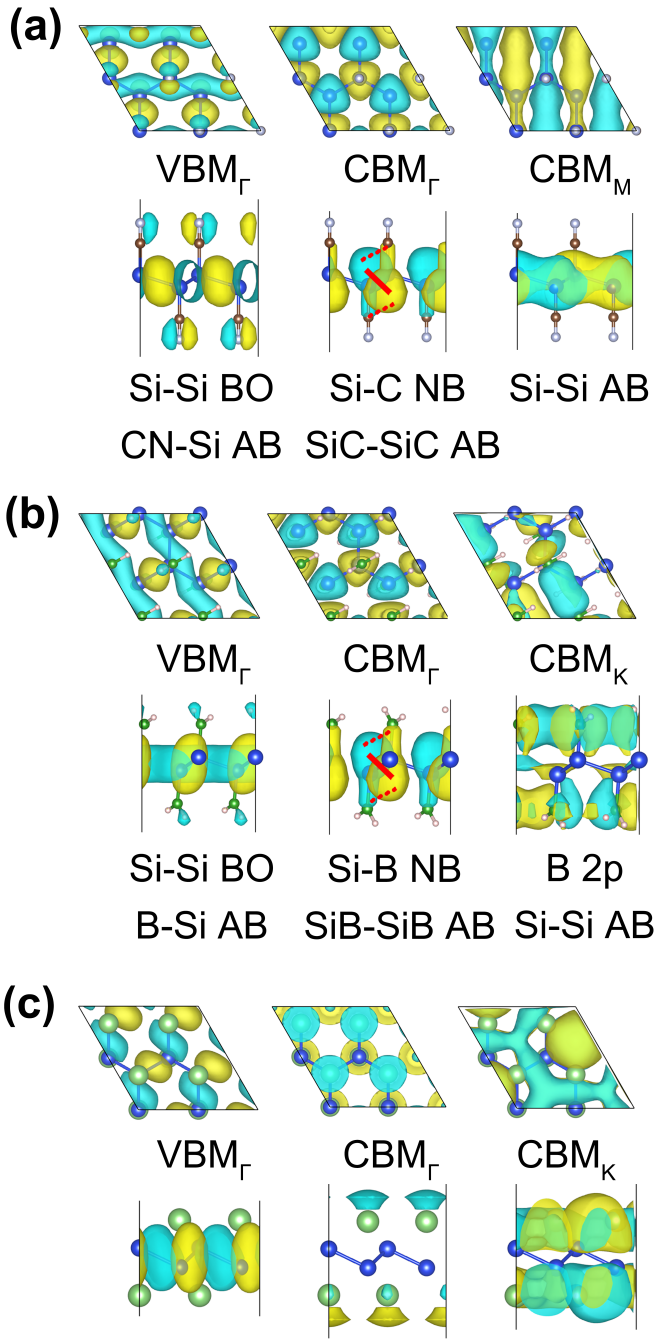

Figure S5. Orbitals at VBM_Γ, CBM_Γ, and CBM_M for (a) SiSH and (b) $SiNH_2$. The characters of the orbitals with respect to certain pairs of atoms are specified: BO = bonding orbital, NB = nonbonding, and AB = antibonding.

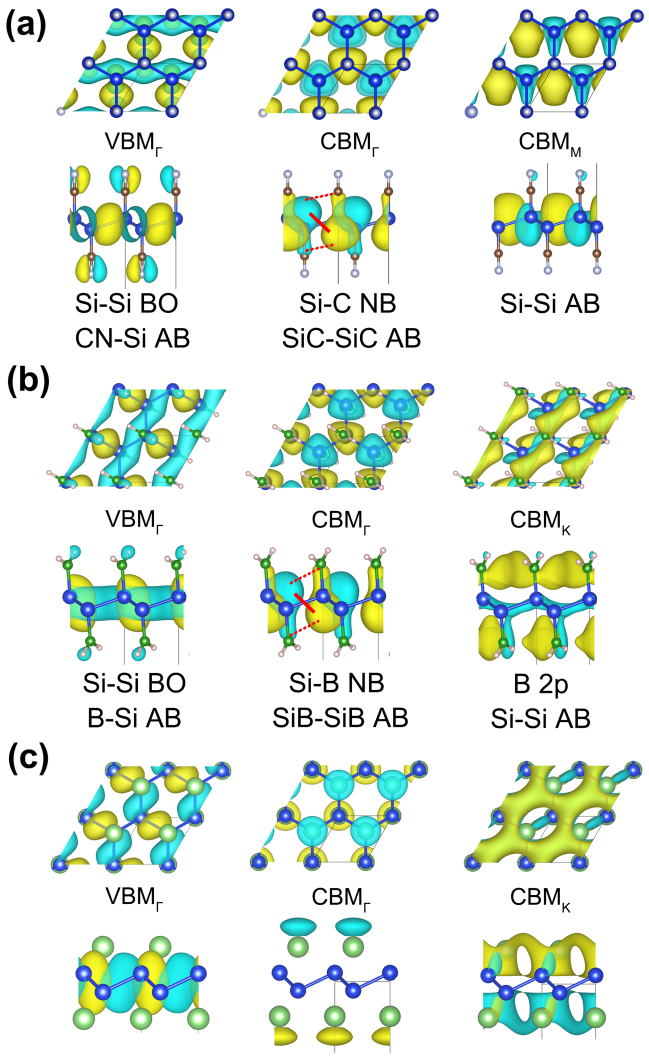

Figure S6. Orbitals at VBM_{Γ}, CBM_{Γ}, and CBM_{M} or CBM_{K} for (a) SiCN and (b) $SiBH_2$, and (c) SiLi. The characters of the orbitals with respect to certain pairs of atoms are specified: BO = bonding orbital, NB = nonbonding, and AB = antibonding.

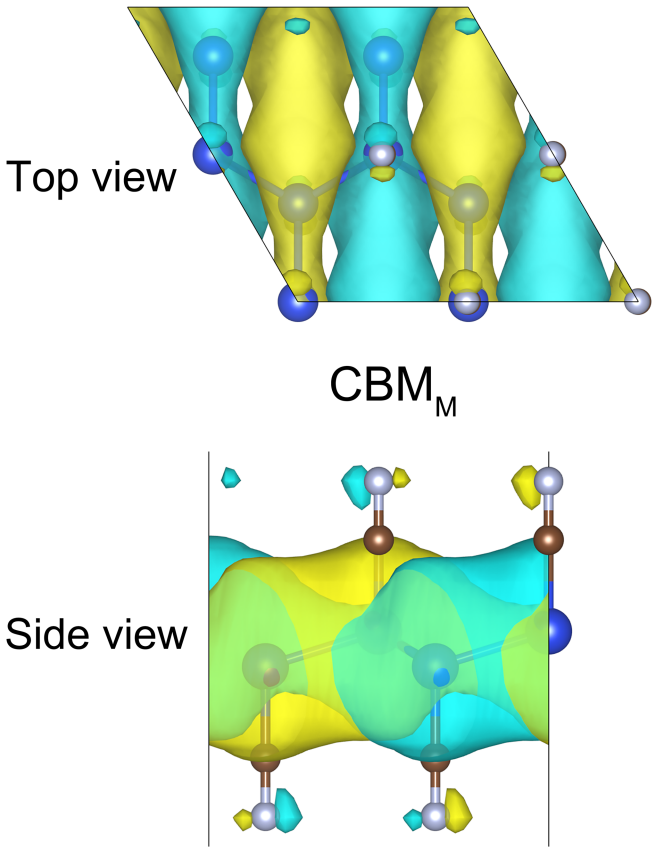

Figure S7. Top and side views of the CBM_M orbital of SiCN, showing the π lobes on the CN ligands. The isovalue is scaled by 4/7 compared to Figure S5(a).

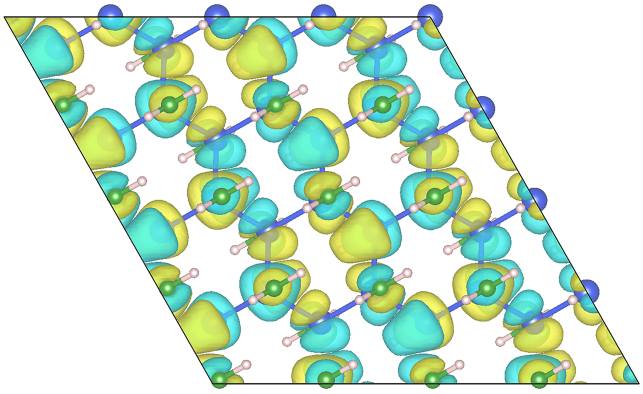

Figure S8. The product of the CBM_{Γ} and CBM_{K} orbitals of $SiBH_2$.

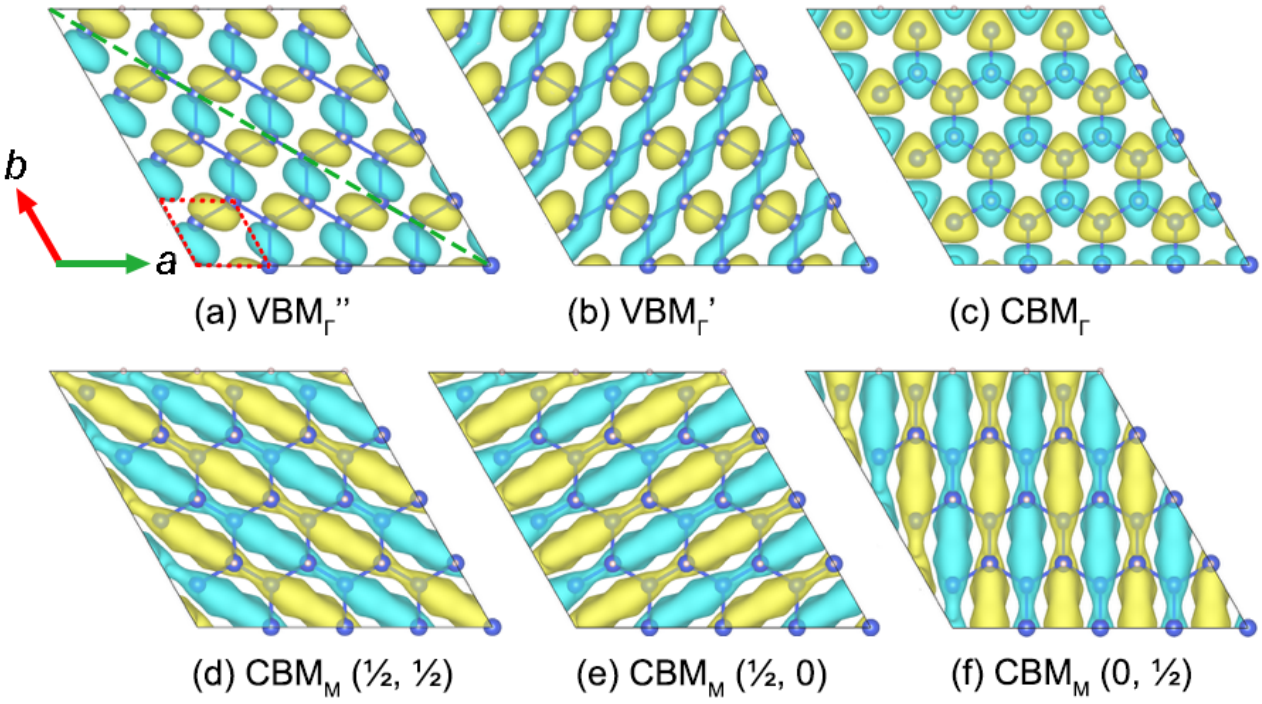

Figure S9. Top views of frontier orbitals of the 4 × 4 × 1 SiH supercell, plotted with an isovalue of ±0.006 a.u. The orbitals are normalized in the supercell. The parenthesized fractions of the CBM_M orbitals indicate their ***k*** vectors in the FBZ of the unit cell. The red dashed lines and the blue dash line in (a) highlight a unit cell and the symmetry plane that cuts through the long diagonal axis of the supercell.

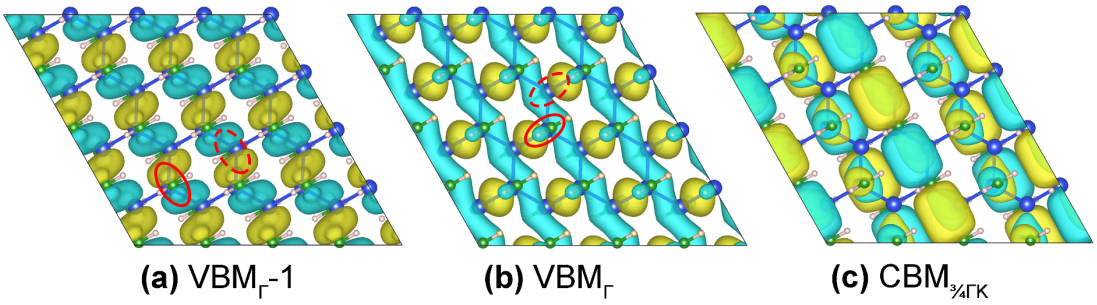

Figure S10. The VBM$_{\Gamma}$-1, VBM$_{\Gamma}$, and CBM$_{¾\Gamma K}$ orbitals of the 4 × 4 × 1 $SiBH_2$ supercell. The solid and dashed ovals in (a) and (b) highlight the bonding interactions above and under the Si framework, and in (b) to highlight the antibonding interactions.

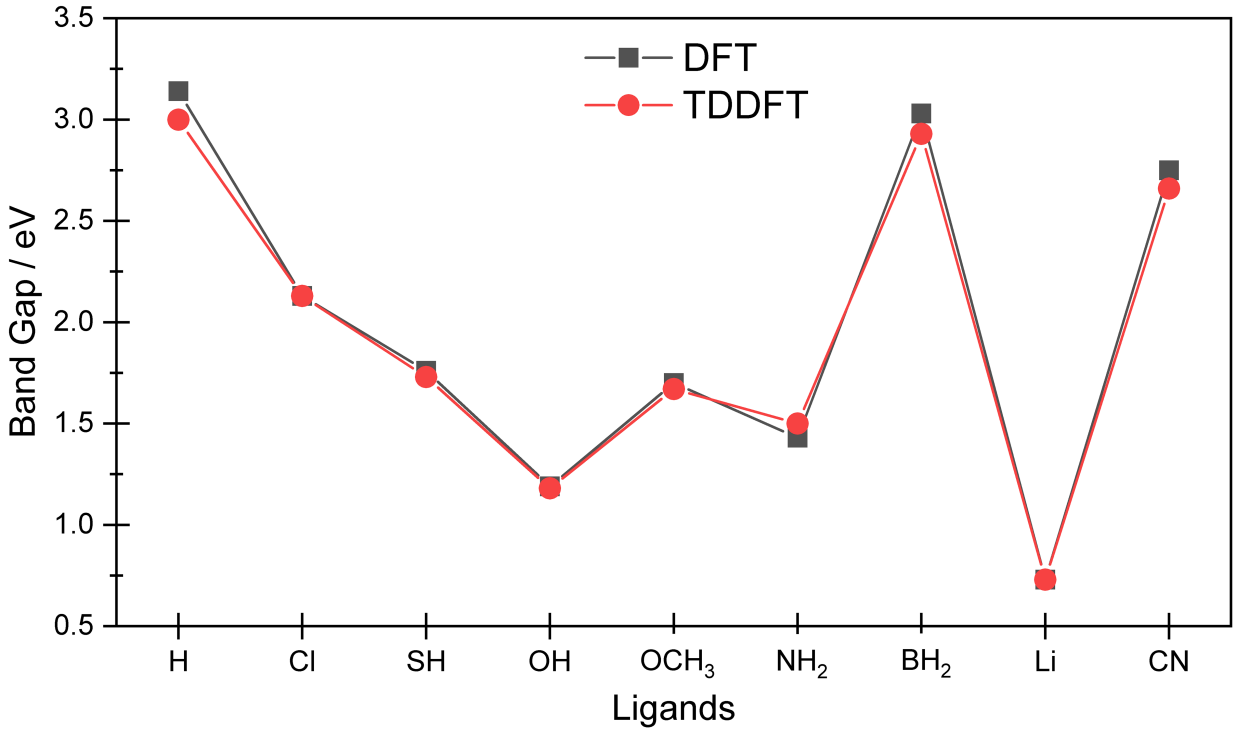

Figure S11. Comparison of DFT and TDDFT band gaps of the SiR species considered in this work.

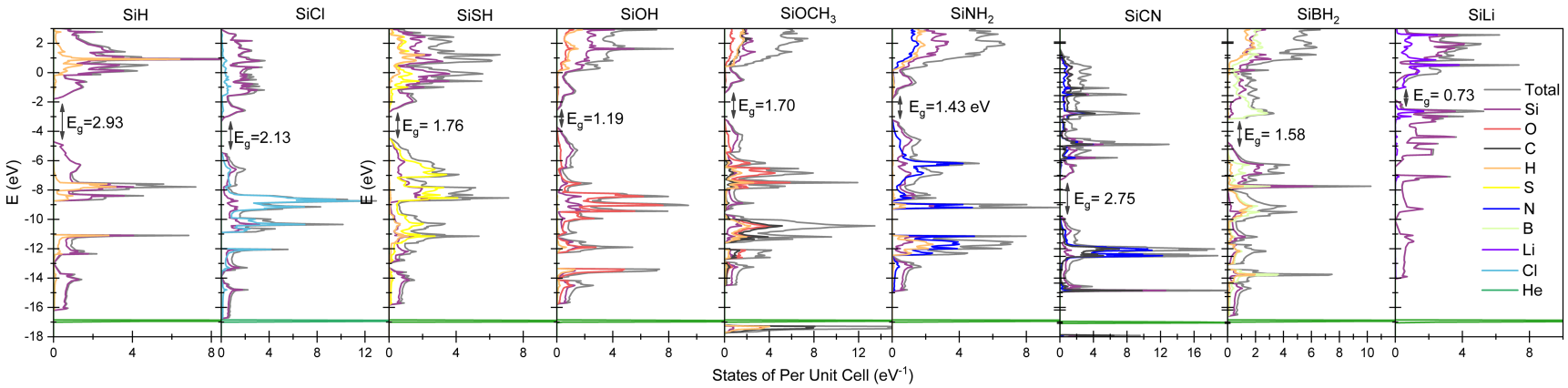

Figure S12. The atom-projected densities of states (pDOSs) for SiR species after orbital energy calibration using a helium atom positioned 20 Å above the layer (see Figure S1 for more details). The DOSs of SiRs are shifted vertically to align their He 1s peaks with the one in the SiH DOS, shown as aligned green peaks at around -17 eV.

Table S1. Summary of the lowest energy optically bright excitation energies and oscillator strengths for the investigated SiR species.

Excitation scheme / System	$VBM_{\Gamma} \rightarrow CBM_{\Gamma}$ (oscillator strength / a.u.)[1]	VBM_{Γ}-1 $\rightarrow CBM_{\Gamma}$ (oscillator strength / a.u.)
SiH	2.99937 (5.36287)	3.00252 (5.35806)
SiCl	2.12708 (1.59969)	2.12826 (1.59694)
SiSH	1.72866 (1.16367)	2.47116 (2.92857)
SiOH	1.18294 (0.731003)	1.41861 (1.29455)
$SiOCH_3$	1.66964 (1.84244)	1.95881 (2.29701)
$SiNH_2$	1.49609 (1.11846)	1.63240 (1.24251)
SiCN	2.66106 (3.75145)	2.66298 (3.79891)
$SiBH_2$	2.93416 (4.72617)	3.18204 (2.75370)
SiLi	2.82772[2] (1.22237)	3.03576[2] (6.44894)

[1] We are aware of the Thomas-Reiche-Kuhn sum rule and know that oscillator strengths shall not be greater than one since their summation should be 1. Here, we just present the oscillator strength results obtained from CP2K calculations, and their large magnitudes arise from the orbital normalization specific to the program package.

[2] The two lowest energy optical excitations of SiLi are from $VBM_{1/2\Gamma M}$ to $CBM_{1/2\Gamma M}$.

Section S2. Electron donating and accepting descriptors for carbon vs. silicon.

Oziminski and Dobrowolski (OD) proposed a set of σ- and π-electron donor-acceptor (sEDA and pEDA) descriptors of typical ligands based on natural population analysis for the ligand-substituted benzenes.[1] The natural populations of the valence σ and π molecular orbitals of a mono-substituted benzene subtract by the populations of the unsubstituted benzene result in good sEDA and pEDA descriptors, respectively. When sEDA > 0 (< 0), it means the σ orbitals of the C_6H_5 moiety have gained (lost) electron population from (to) a σ-donating (-withdrawing) ligand. The same argument applies to pEDA. These descriptors, abbreviated as the OD descriptors, were designed for carbon chemistry. Although the EDA properties are mostly determined by ligands, they are also affected by the system to which the ligands are connected. Therefore, to justify the discussion of the ligands' impact on the band edge energies of the SiR monolayer systems using the well-accepted OD EDA values, we calculated the sEDA and pEDA descriptors for the same comprehensive set of ligands as in OD's study following the same logic but using the Si analogue of benzene as the models.

All EDA-related calculations were performed at the B3LYP/cc-pVTZ level[2-3] using the GAMESS-US program package[4]. The cyclic Si_6H_6 and the substituted Si_6H_5R are buckled, if we fully optimize them. We hence first did a constrained optimization for Si_6H_6, imposing the D_{6h} planar symmetry. Then we replaced one H atom by R ligand, and did another constrained optimization, allowing only the atom(s) on R to relax. The so-optimized Si_6H_6 and Si_6H_5R structures were then used for natural population analysis[5] to obtain the sEDA and pEDA descriptor values of the R ligand. The Si-adapted EDA descriptor (EDA (Si)) values are compiled and compared with the C-adapted analogues (EDA (C)) in

Table S2. The Si-adapted sEDA and pEDA values are plotted against the C-adapted values for a visualized comparison in Figure S13(a) and (b), respectively.

The Li and BeH sEDA (Si) values (labeled by orange markers in Figure S13(a) are much larger than the corresponding sEDA (C) values. With the two data being excluded, a good linear trend line is obtained between sEDA (Si) and sEDA (C) in Figure S13(a). The 0.97 (< 1) slope on one side reflects that Si is more metallic than C and is hence easier to lose electron when connected to a σ-withdrawing ligand. On the other hand, the larger Si_6H_5 ring can accommodate more electron when it is connected to a σ-donating ligand. Li and BeH are so easy to lose electron to the Si_6H_5 ring that they are highly ionic, with +0.85 and +0.59 natural charges, respectively, leading to their exceptionally larger sEDA (Si) values than their sEDA (C) values. Actually, SiLi is a 2D salt, with the Li^+ ions located under (above) the buckled up (down) Si^- ions, opposite to the conventional ligands that are located above (under) the buckled up (down) Si atoms in regular silicanes and form covalent bonds with Si. Very likely, SiBeH is also a similar salt if it is synthesized. In this sense, the Si-Li and Si-BeH interactions are fundamentally different from the other Si-R interactions. It is thus reasonable to exclude the Li and BeH data in fitting the trend lines between the Si- and C-adapted sEDA values and pEDA values.

Table S2. Summary of the Si-adapted sEDA and pEDA descriptor values and their comparison with the C-adapted analogues. Entries are sorted based on the sEDA (Si) values.

Ligand	sEDA (Si)	pEDA (Si)	sEDA (C)	pEDA (C)
F	-0.58	0.04	-0.62	0.08
OMe	-0.56	0.08	-0.50	0.12
OH	-0.54	0.07	-0.56	0.12
NMe_2	-0.52	0.14	-0.48	0.17
OC(=O)Me	-0.52	0.03	-0.55	0.05
NH_2	-0.50	0.12	-0.45	0.15
Cl	-0.30	0.06	-0.26	0.06
Ph	-0.30	0.00	-0.23	0.00
NO_2	-0.30	-0.06	-0.32	-0.07
tBu	-0.27	0.00	-0.24	0.01
$CH=CH_2$	-0.27	-0.01	-0.21	-0.01
Me	-0.26	0.01	-0.23	0.01
CN	-0.24	-0.03	-0.16	-0.04
Br	-0.20	0.06	-0.20	0.06
SH	-0.20	0.09	-0.15	0.09
SMe	-0.19	0.12	-0.13	0.11
NO	-0.18	-0.16	-0.26	-0.13
CF_3	-0.15	-0.01	-0.13	-0.02
COOH	-0.12	-0.05	-0.11	-0.07
CFO	-0.12	-0.06	-0.09	-0.08
$CONH_2$	-0.11	-0.08	-0.14	-0.04
COMe	-0.10	-0.07	-0.12	-0.07
H	0.00	0.00	0.00	0.00
MeSO	0.00	0.01	-0.02	0.02
$MeSO_2$	0.02	-0.01	0.02	-0.02
BH_2	0.12	-0.18	0.17	-0.14
BF_2	0.17	-0.06	0.17	-0.08
SiH_3	0.19	-0.01	0.18	-0.02
$SiMe_3$	0.25	-0.01	0.23	-0.02
BeH	0.68	-0.02	0.40	-0.05
Li	0.87	0.00	0.46	-0.02

A not as good yet satisfactory linear trend line is obtained between the two sets of pEDA values in Figure S13(b). The 1.04 (> 1) slope reflects the overall larger π interactions between the ligands and the benzene ring, which is consistent with the more substantial side-on overlaps for the second period elements than the third period elements. Especially, all the markers that are above the trend line in the first quadrant in Figure S13(b) are for typical π-donors and -acceptors with the second period central atoms N, O, and F. The Si- and C-adapted pEDA values of SH are almost identical, and so are the values of SMe. On one hand, the longer Si-S distance than the C- distance reduces the π interaction. On the other hand, the soft-soft combination between Si and S enhances the π interaction than the hard-soft combination between C and S. These two opposite effects largely cancel each other and hence the pEDA values of SH and SMe are preserved in changing from coordinating to C_6H_5 to coordinating to Si_6H_5. The π -withdrawing (-donating) ligand accommodates (donate) electron pair from (to) its ligated partner through its π empty (lone pair) orbital. It is a typical acid-base interaction, and hence the hard and soft acids and bases (HSAB) theory applies.

Overall, the Si-adapted and C-adapted EDA values correlate well with the close to one slope in the sEDA and pEDA trendlines, except for the highly metallic ligands. Therefore, it is reasonable to use the well-accepted C-adapted EDA descriptors developed by OD to discuss the impacts of the σ- and π-withdrawing/donating capabilities of ligands on the band edge energies of SiR monolayer. Some microscopic deviations between the C- and Si-adapted EDA values are worth further investigation in the future.

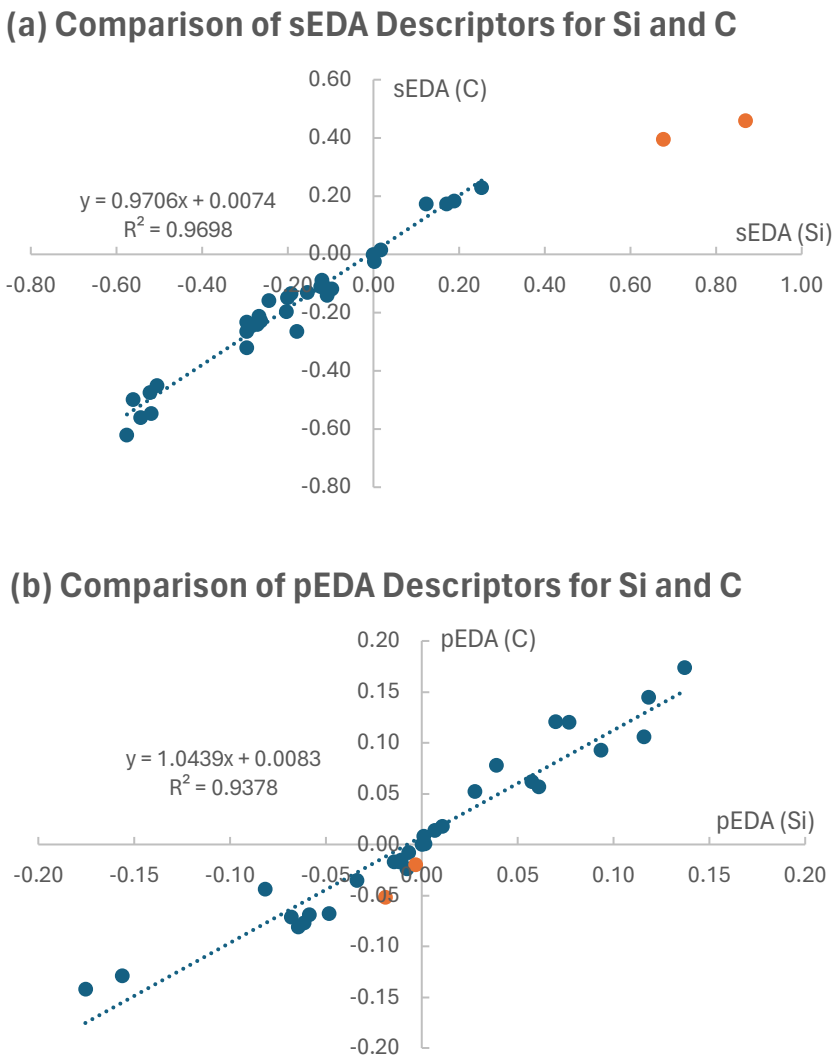

Figure S13. Comparisons of (a) sEDA and (b) pEDA descriptor values obtained for C and Si. The orange markers indicate values for Li and BeH ligands, which are excluded from the trendline fittings.

Section S3. Comparison of TDDFT results of the 4 × 4 × 1 supercell and the 8 × 8 × 1 supercell for SiH.

To investigate the impact of supercell size on the TDDFT calculations, the TDDFT-DOS obtained using the 4 × 4 × 1 and 8 × 8 × 1 supercells for SiH are compared in Figure S14. We emphasize the qualitative nature of the discrete DOS in Figure S14 due to the limited sampling of $\boldsymbol{k}$ vectors in the SiH FBZ. The true DOS must be continuous as the VB and CB are continuous below and above their respective band edges. In the 4 × 4 × 1 supercell calculation, the lowest optically bright state lies at 3.0 eV, while in the 8 × 8 × 1 supercell calculation, the lowest optically bright state is 0.23 eV higher. In addition, the number of sampled $\boldsymbol{k}$ vectors is increased due to the expansion of the supercell, and the inclusion of the $\frac{1}{4}$ΓM and $\frac{3}{4}$ΓM $\boldsymbol{k}$ points increase the number of excited states in the originally blank range of 3.4 – 4.0 eV. In general, more states are present to fill the energy range above the lowest excitation energy than in Figure S14(a). The optical absorption must also be continuous in reality: given the bright transitions from VBM_{Γ} to CBM_{Γ} and from $VBM_{½\Gamma M}$ to $CBM_{½\Gamma M}$ in Figure S14(a), very naturally, all continuous VB-to-CB $\boldsymbol{k}$-conserved transitions along the Γ-to-M path are bright transitions. This is however not reflected in Figure S14(b), since the additional optically bright $VBM_{1/4\Gamma M}$-to-$CBM_{1/4\Gamma M}$ transition occurs at very similar energy as the $VBM_{½\Gamma M}$-to-$CBM_{½\Gamma M}$ transition, and hence their absorption peaks overlap (labeled by ⑩ in Figure S14(b)). As the supercell is further enlarged, the continuous absorptions will be captured. The explanation on the splitting of the VBM_{Γ}-to-CBM_{M} states applies to all states with hole on VBM_{Γ}×2 and particle on the Γ-to-M CBM path (except CBM_{Γ}), e.g., the splittings of the ②, ③, ④, and ⑧ states in Figure S14(b).

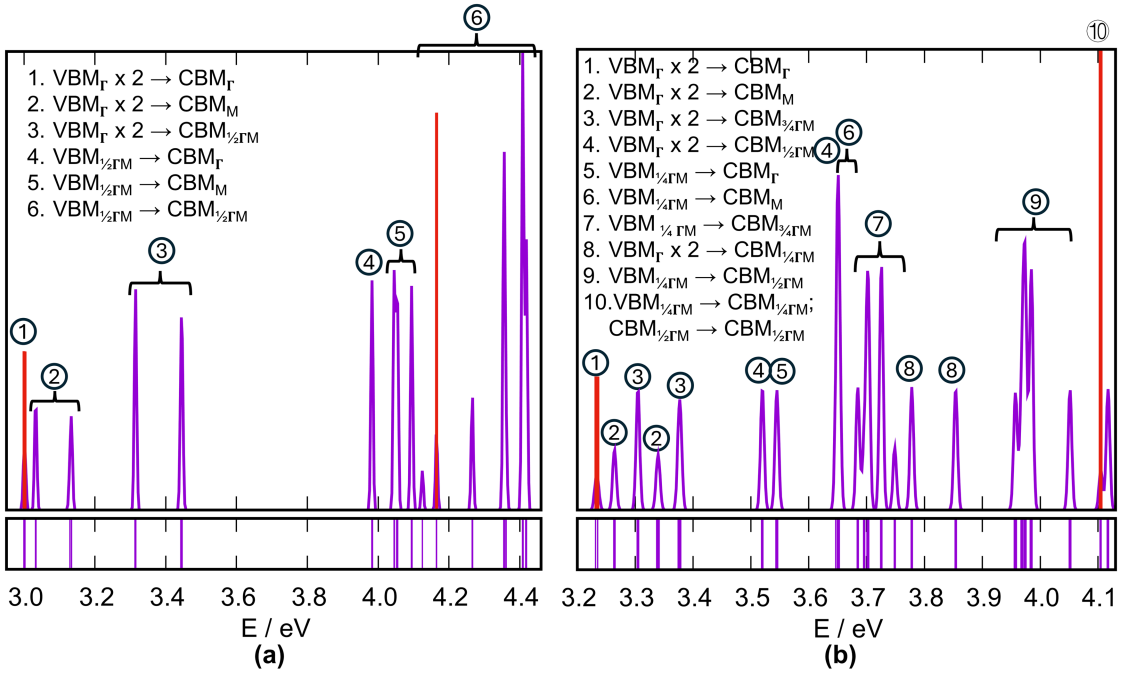

Figure S14. TDDFT-DOS of SiH obtained using (a) the 4 × 4 × 1 supercell and (b) the 8 × 8 × 1 supercell. The oscillator strengths are plotted as red spikes. The TDDFT-DOS are obtained with Gaussian broadening of each state's spike in the lower minor panels using the broadening parameter $\sigma = 0.007$ eV and summing all the Gaussians. States that arise from the same set of hole and particle orbitals are grouped and labeled by circled numbers. The two panels do not share the same labels for the same states. The hole and particle orbitals that dominate the labeled groups of states are given. "VBMΓ×2" indicates the doubly degenerate VBM orbitals at Γ. In the lower minor panels, spikes of equal heights are drawn at calculated the excitation energies, indicating the existence of states at specific energies.

Section S4. Band edge energies as empirical functions of σ- and π-electron donor-acceptor descriptors of ligands.

In the Results and Discussions section in the main text, we have qualitatively explained the dependences of VBM and CBM energies of the SiR species on the σ- and π-withdrawing/donating capabilities of the R ligands. It is tempting to develop analytical empirical functions to describe these dependencies. Since silicane is prone to oxidation, and those oxidative ligands are often simultaneous σ-withdrawers and π-donors, we are especially interested in the functions for σ-withdrawing and π-donating ligands. We set a function

$$f(x,y) = E_{VBM(H)} + a(\cos\theta\, x + \sin\theta\, y) + b(-\sin\theta\, x + \cos\theta\, y) + c(\cos\theta\, x + \sin\theta\, y)^2 + d(-\sin\theta\, x + \cos\theta\, y)^2$$

where x and y are the sEDA and pEDA values proposed by Oziminski and Dobrowolski,[1] $E_{VBM(H)}$ the VBM energy of SiH, and θ, a, b, c, d the fitting parameters. θ is the angle that rotates x and y to new coordinates. The other four parameters are expansion coefficients of the linear and quadratic terms of the new coordinates. Since x and y are unitless variables, the parameters a to d have the same eV unit as the VBM energies. Since we have rotated the coordinates, there is no need to include the bilinear term. For H, $x = y = 0$, and therefore, $f(0,0) = E_{VBM(H)}$. The VBM energy of SiH is hence not a datum for fitting. We fit the function using the VBM energies of SiR with R = Cl, OH, OCH_3, SH, and NH_2, and the x and y values of the ligands. The resultant parameters are $\theta = 1.3706, a = 194.095, b = -14.877, c = -2613.28, d = 24.996$. The fitted function and the data are plotted in Figure S15(a).

Given the same numbers of parameters and data, the fitting has zero residual. This certainly does not mean that the resultant function is perfect. It simply reflects the limitation of data set for

the fitting. The purpose of our fitting is more to inspire future studies to develop such an analytical empirical function. Also, for ligands whose σ- and π-donating/withdrawing indices are similar to those of the five ligands included for the fitting, we may use the current function to estimate the VBM energy.

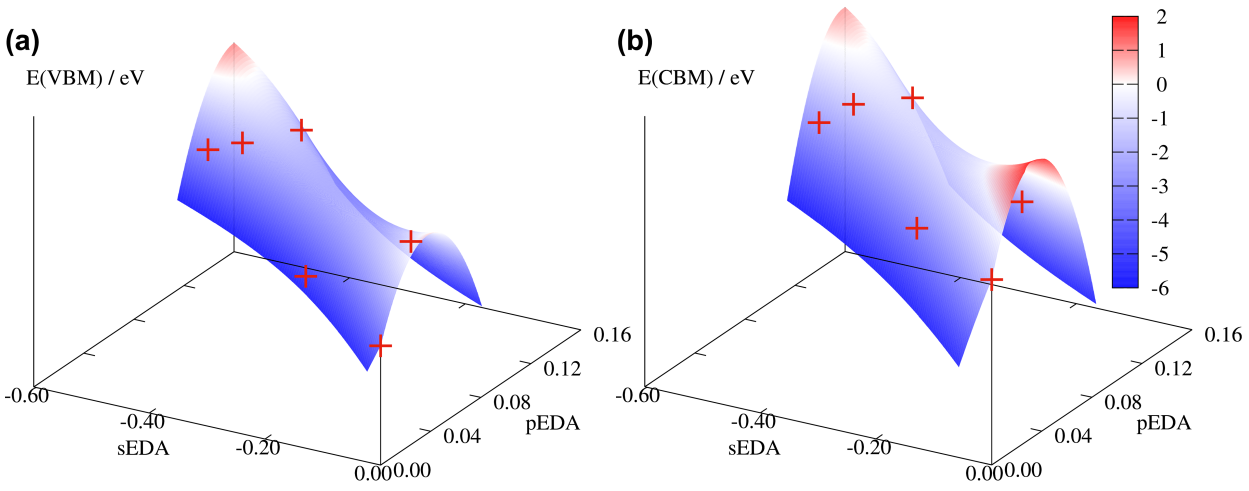

Figure S15. The fitted function (the surface) and the fitted data (red markers) for (a) the VBM and (b) the CBM energies of the SiR species with σ-withdrawing and π-donating R ligands.

We performed a similar fitting for the CBM energies with the $E_{VBM(H)}$ being replaced by $E_{CBM(H)}$ in the fitting function. The resultant parameters are $\theta = 1.3685, a = 242.098, b = -19.264, c = -3544.81, d = 27.185$. The fitted function and the data are plotted in Figure S15(b). The independent fittings for the VBM and CBM energies resulted in essentially the same θ value. This suggests that the two coordinates:

$$x' = 0.20x + 0.98y; y' = 0.98x - 0.20y$$

are natural coordinates to describe the VBM and CBM energies of SiR with σ-withdrawing and π-donating R ligand. There is a statistical reason for the specific natural coordinates. The OD

pEDA descriptor values are plotted against the sEDA descriptor values in Figure S16 for the simultaneous σ-withdrawing and π-donating ligands included in OD's work. Clearly, the distribution of the data follows several parallel lines with the slope of -0.2, which is consistent with the θ angle. Again, a larger set of data are needed for more convincing fittings and also a more reliable intrinsic θ angle that gives the natural coordinates for the sWpD ligands.

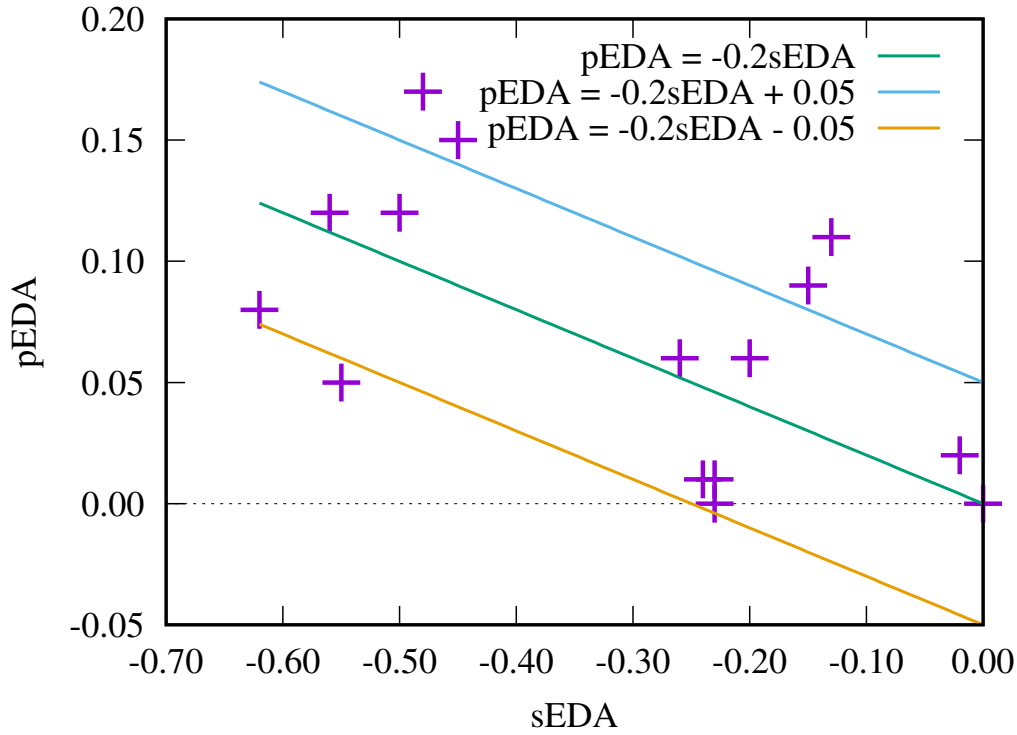

Figure S16. Plotting of the pEDA against the sEDA descriptor values proposed by OD for the simultaneous σ-withdrawing and π-donating ligands included in Ref.[1] and a few parallel lines that demonstrate the distribution of the data.

We expanded the data set to include the other ligands that do not fall in the quadrant of being simultaneous σ-withdrawers and π-donors, i.e., SiCN and $SiBH_2$. SiLi is excluded since this 2D salt is fundamentally different from the rest covalent silicanes. The fitting of the VBM energies gave: $\theta = 1.22193, a = 20.933, b = -6.835, c = -191.273, d = 24.500$, with the root mean

square of residuals being 0.51 eV. The fitting of the CBM energies gave: $\theta = 1.27648, a = 13.389, b = -8.079, c = -352.714, d = 17.335$, with the root mean square of residuals being 0.50 eV. Again, similar θ parameters were obtained to rotate the x and y coordinates in the two independent fittings. We think of these two functions as being inferior to the two above fitted for one specific type of ligands. The differences between the different types of ligands shall not be ignored, especially using such a low order polynomial expansion as the fitting function. At presence, we have only one datum for the σ-withdrawing and π-withdrawing quadrant, and also one datum for the σ-donating and π-withdrawing quadrant, which are not enough to support any fitting in each of the quadrant. More data in the two quadrants are needed for future fittings for their individual fittings.

References

1. Ozimiński, W. P.; Dobrowolski, J. C., σ- and π-electron contributions to the substituent effect: natural population analysis. *J. Phys. Org. Chem.* **2009,** *22* (8), 769-778.
2. Stephens, P. J.; Devlin, F. J.; Chabalowski, C. F.; Frisch, M. J., Ab Initio Calculation of Vibrational Absorption and Circular Dichroism Spectra Using Density Functional Force Fields. *J. Phys. Chem. C* **1994,** *98* (45), 11623-11627.
3. Dunning, T. H., Jr., Gaussian basis sets for use in correlated molecular calculations. I. The atoms boron through neon and hydrogen. *J. Chem. Phys.* **1989,** *90* (2), 1007-1023.
4. Barca, G. M. J.; Bertoni, C.; Carrington, L.; Datta, D.; De Silva, N.; Deustua, J. E.; Fedorov, D. G.; Gour, J. R.; Gunina, A. O.; Guidez, E.; Harville, T.; Irle, S.; Ivanic, J.; Kowalski, K.; Leang, S. S.; Li, H.; Li, W.; Lutz, J. J.; Magoulas, I.; Mato, J.; Mironov, V.; Nakata, H.; Pham, B. Q.; Piecuch, P.; Poole, D.; Pruitt, S. R.; Rendell, A. P.; Roskop, L. B.; Ruedenberg, K.; Sattasathuchana, T.; Schmidt, M. W.; Shen, J.; Slipchenko, L.; Sosonkina, M.; Sundriyal, V.; Tiwari, A.; Galvez Vallejo, J. L.; Westheimer, B.; Włoch, M.; Xu, P.; Zahariev, F.; Gordon, M. S., Recent developments in the general atomic and molecular electronic structure system. *J. Chem. Phys.* **2020,** *152* (15), 154102.
5. Reed, A. E.; Weinstock, R. B.; Weinhold, F., Natural population analysis. *J. Chem. Phys.* **1985,** *83* (2), 735-746.